Self-sustained flow-oscillations in hole-tone problem (Mathematical Physics and Applications of Nonlinear Wave Phenomena)

AUTHOR(S):

Langthjem, Mikael A.; Nakano, Masami

数理解析研究所講究録
第1594巻 2008年 18-33

Self-sustained flow-oscillations in hole-tone problem

Mikael A. Langthjem†, Masami Nakano‡

†Faculty of Engineering, Yamagata University, Jonan 4-chome, Yonezawa-shi, 992-8510 Japan

‡Institute of Fluid Science, Tohoku University, 2-1-1 Katahira, Aoba-ku, Sendai-shi, 980-8577 Japan

Abstract

A method for simulating the hole-tone feedback cycle (Rayleigh's bird-call), based on a three-dimensional discrete vortex method, is described in detail. Evaluation of the sound generated by the self-sustained flow oscillations is based on the Powell-Howe theory of vortex sound and the boundary element method. Emphasis is placed on the development of a model for the coupling between the vortex-dominated main flow and the acoustic field. The final part of the paper considers, briefly, an analysis based on the method of proper orthogonal decomposition.

Keywords: aeroacoustics; self-sustained flow oscillations; three-dimensional vortex method; vortex sound; boundary element method; proper orthogonal decomposition

1 Introduction

Self-sustained fluid oscillations can occur in a variety of practical applications where a shear layer impinges upon a solid structure [16, 17]. The present paper is concerned with such oscillations in the hole-tone problem [15, 2], where a fluid jet issuing from a circular hole in a plate (or from a nozzle) impinges upon a (second) plate with a similar hole, located a little downstream from the nozzle. Self-sustained oscillations of the jet are generated, accompanied by sound with a definite tone. The common teakettle whistle and the bird-call[1] is an example of utilization of the phenomenon.

In his *Theory of Sound* [15] Rayleigh explained the basic mechanism as follows: "When a symmetrical excrescence reaches the second plate, it is unable to pass the hole with freedom, and the disturbance is thrown back, probably with the velocity of sound, to the first plate, where it gives rise to a further disturbance, to grow in its turn during the progress of the jet."

The system is thus one where the sound generation is caused by *synchronization* [14] between the sound-generating flow and the acoustic field.

The dominating frequency f_0 satisfies the criterion

$$\ell/u_c + \ell/c_0 = n/f_0, \tag{1}$$

where ℓ is the length of the gap between the nozzle exit and the end plate, u_c is the vortex convection velocity ($u_c \approx 0.6u_0$, where u_0 is the mean flow velocity), c_0 is the speed of sound, and n is a mode number which may take the values $\frac{1}{2}, 1, \frac{3}{2}, \ldots$. A change in the value of n implies a corresponding 'jump' in the frequency f_0.

[1] A whistle used to simulate natural bird calls.

A number of experimental studies on the hole tone problem have been published; particularly noteworthy is the comprehensive work of Chanaud & Powell [2]. Theoretical and numerical studies are however few. A large body of work has been done on the related, two-dimensional edge-tone problem; some parallels between the two problems are drawn in Ref. [2].

As explained in an earlier paper [8], one of the main purposes of this work is to investigate the effects of non-axisymmetric flow disturbances, imposed 'mechanically', in the experiments via piezoelectric actuators placed around the circumference inside the nozzle. In the numerical computations, this is simulated via a deformable nozzle. A three-dimensional formulation is thus necessary. The forcing (control) problem will be considered in a future paper. In this paper the numerical method will be described in detail in Sections 2-3. A numerical example will be presented in Section 4. Finally, an analysis based on the method of proper orthogonal decomposition will be described briefly in Section 5.

2 The discrete vortex flow model

2.1 Vortex filament model of the jet flow

The shear layer of the jet issuing from the nozzle is represented by discrete vortex rings. These rings will be disturbed mechanically at the nozzle exit such that they loose their natural axisymmetric form, and are thus represented by three-dimensional vortex filaments. The induced velocity $\mathbf{u}_{\text{fv}} = (u_1, u_2, u_3)_{\text{fv}}$, at position $\mathbf{x} = (x_1, x_2, x_3)_i$ and time t, from N_{fv} vortex rings represented by the space curves $\mathbf{r}_j(\xi, t)$, is obtained from the generalized Biot-Savart law [9]

$$\mathbf{u}_{\text{fv}}(\mathbf{x}, t) = -\sum_{j=1}^{N_{\text{fv}}} \frac{\Gamma_j}{4\pi} \oint_{C_j(\xi)} \frac{\{\mathbf{x} - \mathbf{r}_j(\xi, t)\} \times \partial \mathbf{r}_j / \partial \xi \; q\left(|\mathbf{x} - \mathbf{r}_j(\xi, t)|/\sigma_j\right)}{|\mathbf{x} - \mathbf{r}_j(\xi, t)|^3} d\xi. \tag{2}$$

Here Γ_j is the strength (circulation) of the j'th vortex ring and $C_j(\xi)$ its contour, described by the parameter ξ. The 'smoothing function' $q(y)$ represents the structure of the vortex core, with $\sigma_j(\xi, t)$ being the core radius. It eliminates the logarithmic singularity at $\mathbf{x} = \mathbf{r}_j$, and smoothes out the vorticity distribution. In the present work the Rosenhead-Moore function

$$q(\kappa) = \frac{\kappa^3}{(\kappa^2 + \alpha)^{\frac{3}{2}}} \tag{3}$$

is chosen [9]. If (2) and (3) are to give the same single-ring speed as the Gaussian core distribution

$$\varpi(\varrho) = \pi^{-\frac{3}{2}} \exp(-\varrho^2), \tag{4}$$

with the corresponding smoothing function

$$q(\kappa) = 4\pi \int_0^{\kappa} \varpi(\varrho) \varrho^2 d\varrho, \tag{5}$$

then the parameter α should have the value 0.413 [1]. This value is accordingly used in the numerical simulations.

2.2 Representation of solid surfaces

The solid surfaces are represented by rectilinear vortex ring 'panels', made up of four straight vortex filaments, as indicated in Fig. 1. The velocity induced from such a vortex panel can be obtained by evaluating the integral in (2), with $q \equiv 1$, along the line segments between $\mathbf{y}_j$ and

$\mathbf{y}_{j+1}$, $j = 1, \ldots, 4$, where $\mathbf{y}_5 := \mathbf{y}_1$. Following the approach of Katz & Plotkin [6], the velocity induced from N_{bv} panels is

$$\mathbf{u}_{\text{bv}}(\mathbf{x}) = \sum_{j=1}^{N_{\text{bv}}} \sum_{i=1}^{4} \frac{\Gamma_j}{4\pi} \left[\frac{\mathbf{r}_i \times \mathbf{r}_{i+1}}{|\mathbf{r}_i \times \mathbf{r}_{i+1}|^2} \mathbf{r}_0 \cdot \left(\frac{\mathbf{r}_i}{r_i} - \frac{\mathbf{r}_{i+1}}{r_{i+1}} \right) \right]_j, \tag{6}$$

where $\mathbf{r}_i = \mathbf{y}_i - \mathbf{x}$ and $\mathbf{r}_0 = \mathbf{r}_i - \mathbf{r}_{i+1}$ (and $\mathbf{r}_5 := \mathbf{r}_1$). The mean jet flow is also provided by a number of such vortex panels, placed on the 'back' of the nozzle tube, and by a single point source, which provides the induced velocity

$$\mathbf{u}_{\text{ps}}(\mathbf{x}) = \frac{\sigma}{4\pi} \frac{\mathbf{r}}{r^3}. \tag{7}$$

Here σ is the source strength, $\mathbf{r} = \mathbf{x} - \mathbf{y}$ and $r = |\mathbf{r}|$. The velocity at an arbitrary point $\mathbf{x}$ is thus given by

$$\mathbf{u}(\mathbf{x}) = \mathbf{u}_{\text{fv}} + \mathbf{u}_{\text{bv}} + \mathbf{u}_{ps}. \tag{8}$$

The strengths of the bound vortex panels, and the single point source, are dictated by the boundary conditions and the mean jet velocity.

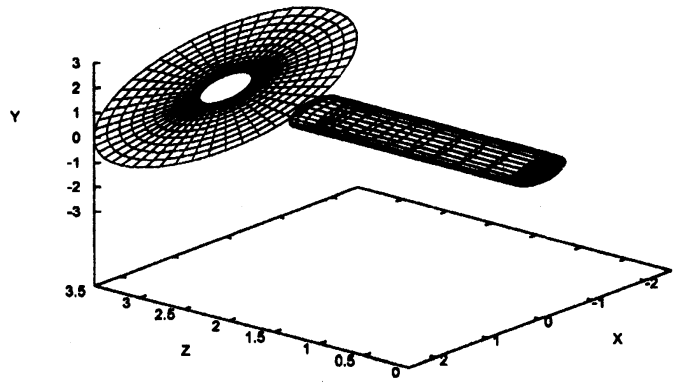

Figure 1: Solid surfaces represented by vortex panels. The mean flow-generating panels are placed at z = 0.0, the nozzle exit at z = 2.5, and the end plate at z = 3.5.

First, it is required that the inviscid boundary condition of zero normal velocity is satisfied on the exit pipe ('surface 2') and the end plate ('surface 3'), i.e.

$$u_n(\mathbf{x}_{i,j}^{\text{cp}k}) = 0, \quad i = 1, \ldots, N_{\theta k}, \quad j = 1, \ldots, N_{rk}, \quad k = 2, 3, \tag{9}$$

where $\mathbf{x}_{i,j}^{\text{cp}k}$ are control points located in the center of the vortex panels, $N_{\theta k}$ is the number of panels in circumferential direction, and N_{rk} the number of panels in radial direction.

Second, the velocity distribution on the mean flow-providing upstream end of the exit pipe ('surface 1') is required to be uniform. This is obtained by the following two conditions:

$$u_n(\mathbf{x}_{i,j}^{\text{cp1}}) - u_n(\mathbf{x}_{i+1,j}^{\text{cp1}}) = 0, \quad i = 1, \ldots, N_{\theta 1} - 1, \quad j = 1, \ldots, N_{r1}, \tag{10}$$

$$u_n(\mathbf{x}_{i,j}^{\text{cp1}}) - u_n(\mathbf{x}_{i,j+1}^{\text{cp1}}) = 0, \quad i = N_{\theta 1} - 1, \quad j = 1, \ldots, N_{r1}. \tag{11}$$

Equation (10) expresses a zero velocity jump across any two adjacent panels in radial direction, at any circumferential station. Equation (11) expresses a zero velocity jump across any two adjacent panels in circumferential direction, for one particular radius.

The third and final condition is the specification of the mean velocity at a specified point $\mathbf{x}_*$;

$$u_3(\mathbf{x}_*) = u_0. \tag{12}$$

The conditions (9)-(12) constitute $\sum_k (N_{\theta k} \times N_{rk}) + 1$ equations with the same number of unknowns. The matrix equation system corresponding to these equations takes the form

$$\mathbf{A}\boldsymbol{\Gamma} = \mathbf{b}. \tag{13}$$

Here the matrix $\mathbf{A}$ contains the influence coefficients and $\boldsymbol{\Gamma}$ the unknown vortex/source strengths. The vector $\mathbf{b}$ contains the induced velocities from the free vortices; the elements are given by

$$b_j = -\sum_{i=1}^{N_{\rm fv}} \mathfrak{F}\{\mathbf{u}_{\rm fv}\}, \tag{14}$$

where $\mathfrak{F}\{\ \}$ represents the 'operations' defined by (9)-(12).

2.3 Vortex shedding mechanism

The rate of continuous shedding of circulation γ from the nozzle is given by

$$\frac{d\gamma}{dt} = \tfrac{1}{2}\left(u_{t-}^2 - u_{t+}^2\right), \tag{15}$$

where u_{t-} is the (tangential) velocity at the pipe exit, $z_{\rm exit}$ say, on the inner surface, and u_{t+} is the corresponding velocity on the outer surface. This equation can be obtained by integrating the tangential component of the Euler equations over the tube surface, and using the Kutta condition, which demands that the pressure a little above the nozzle edge equals the pressure a little below.

In the simulation a vortex ring is released at every time-step, at the position

$$z_{\rm rel} = z_{\rm exit} + \tfrac{1}{2}\Delta t\left(u_{t-} + u_{t+}\right). \tag{16}$$

Its strength is obtained from (15) as

$$\Gamma = \tfrac{1}{2}\Delta t\left(u_{t-}^2 - u_{t+}^2\right). \tag{17}$$

The vortex rings, described by the space curves $\mathbf{r}_j(\xi,t)$, are discretized by employing $N_{\rm mp}$ marker points on each curve, connected via cubic splines. The positions of the marker points on the shed vortex rings, described by the vectors $\mathbf{r}_m(\zeta_n,t)$, are updated by solving numerically the system of ordinary differential equations

$$\begin{aligned}\frac{d\mathbf{r}_m(\zeta_n,t)}{dt} &= -\sum_{j=1}^{N_{\rm fv}} \frac{\Gamma_j}{4\pi} \oint_{C_j(\xi)} \frac{\{\mathbf{r}_m(\zeta_n,t) - \mathbf{r}_j(\xi,t)\} \times \partial \mathbf{r}_j/\partial\xi}{\{|\mathbf{r}_m(\zeta_n,t) - \mathbf{r}_j(\xi,t)|^2 + \alpha\sigma_j^2(\xi,t)\}^{\frac{3}{2}}} d\xi \\ &+ \mathbf{u}_{\rm bv}(\zeta_n,t) + \mathbf{u}_{\rm ps}(\zeta_n,t), \qquad m = 1,\ldots,N_{\rm fv}, \quad n = 1,\ldots,N_{\rm cp}.\end{aligned} \tag{18}$$

To this end the fourth-order Runge-Kutta method is applied. The integrations over $C_j(\zeta)$ in (18) are carried out using Gaussian quadrature [7].

Except for the viscous effect simulated by the Kutta condition, the computations are basically inviscid. This means that the vortex rings keep their strengths throughout the simulation, once released. The volume of each individual ring must thus be kept constant; this constraint is imposed via the equations

$$\frac{d}{dt}(\sigma_n^2 \ell_n)_m = 0, \quad n = 1,\ldots,N_{\rm cp}, \quad m = 1,\ldots,N_{\rm fv}, \tag{19}$$

where ℓ_n is the instantaneous length of the n'th filament.

Finally, it must be mentioned that, following an advice of Leonard [9], the core radius σ_j in (18) is replaced by $\frac{1}{2}\left(\sigma_m^2 + \sigma_j^2\right)^{1/2}$. This symmetric form will preserve linear and angular momentum.

3 Aeroacoustic model

3.1 The equation of vortex sound and its formal solution in terms of integral equations

To evaluate the sound generated by the self-sustained flow oscillations, the start point is taken in Howe's equation for vortex sound at low Mach numbers [5]. Here the sound pressure $p(\mathbf{x},t)$ is related to the vortex force $\mathbf{L}(\mathbf{x},t) = \boldsymbol{\omega}(\mathbf{x},t) \times \mathbf{u}(\mathbf{x},t)$ via the non-homogeneous wave equation

$$\left(\frac{1}{c_0^2}\frac{\partial^2}{\partial t^2} - \nabla^2\right) p = \rho \nabla \cdot \mathbf{L}, \tag{20}$$

where the vorticity $\boldsymbol{\omega} = \nabla \times \mathbf{u}$. The boundary conditions are

$$\frac{\partial p}{\partial n} = 0 \text{ on the end plate}, \quad p \to 0 \text{ for } |\mathbf{x}| \to \infty, \tag{21}$$

where n denotes the outward normal vector.

Fourier transform with respect to time t and frequency ν are defined as

$$P(\mathbf{x},\nu) = \frac{1}{2\pi}\int_{-\infty}^{\infty} p(\mathbf{x},t)\mathrm{e}^{\mathrm{i}\nu t}dt, \qquad p(\mathbf{x},t) = \int_{-\infty}^{\infty} P(\mathbf{x},\nu)\mathrm{e}^{-\mathrm{i}\nu t}d\nu. \tag{22}$$

Applying the first of the equations (22) to (20) gives

$$\left(\nabla^2 + k^2\right) P = -\rho \nabla \cdot \mathfrak{L} \tag{23}$$

where $\mathfrak{L}(\mathbf{x},\nu)$ is the Fourier transform of $\mathbf{L}(\mathbf{x},t)$, and $k = \nu/c_0$ is the wave number. To solve (23) use is made of the free-space Green's function

$$G(\mathbf{x},\mathbf{y}) = \frac{\mathrm{e}^{\mathrm{i}kr}}{4\pi r}, \quad r = |\mathbf{x}-\mathbf{y}| \tag{24}$$

which is a solution of the equation

$$\left(\nabla^2 + k^2\right) G = -\delta(\mathbf{x}-\mathbf{y}), \tag{25}$$

and which satisfies the second of the boundary conditions (21). The function $\delta(\mathbf{x}-\mathbf{y})$ is the delta function. Here and in the sequel, $\mathbf{x}$ denotes the location of an observation point and $\mathbf{y}$ the location of an acoustic source.

Multiplying (23) by G and (25) by P gives, after integration and use of Green's second identity,

$$\begin{aligned} \varsigma P(\mathbf{x},\nu) &= \rho \iiint G(\mathbf{x},\mathbf{y})\, \nabla_{\mathbf{y}} \cdot \mathfrak{L}(\mathbf{y},\nu)\, d^3\mathbf{y} \\ &- \iint \left[G(\mathbf{x},\mathbf{y}_\beta)\frac{\partial}{\partial n_\beta} P(\mathbf{y}_\beta,\nu) - P(\mathbf{y}_\beta,\nu)\frac{\partial}{\partial n_\beta} G(\mathbf{x},\mathbf{y}_\beta)\right] d^2\mathbf{y}_\beta. \end{aligned} \tag{26}$$

The subscript $\mathbf{y}$ on the del-operator in the first term on the right hand side indicates differentiation with respect to the source coordinates $\mathbf{y}$. The subscript α on $\mathbf{y}_\beta$ indicates a point on the end plate and n_β the normal vector at that point. The notation $d^3\mathbf{y}$ is used for $dy_1 dy_2 dy_3$ and $d^2\mathbf{y}_\beta$ for $dy_{\beta 1} dy_{\beta 2}$. The parameter ς is given by [13]

$$\varsigma = \begin{cases} 1 & \text{when } \mathbf{x} \text{ is in the acoustic medium,} \\ \frac{1}{2} & \text{when } \mathbf{x} \text{ is on a solid boundary,} \\ 0 & \text{when } \mathbf{x} \text{ is outside the acoustic medium.} \end{cases} \tag{27}$$

The first of the equations (21) gives that $\partial P/\partial n_\beta = 0$.

The first term on the right hand side of (26) can, via integration by parts, be rewritten as

$$-\iiint \frac{\partial G}{\partial y_j}\,\mathfrak{L}_j\,d^3\mathbf{y}. \tag{28}$$

In this equation and in the sequel, summation over repeated *latin* indices is to be understood. [Summation is not carried out over repeated greek indices.]

Considering a plate of vanishing thickness, Terai [19] has shown that the pressure at a point $\mathbf{x}$ away from the plate can be expressed as

$$P(\mathbf{x},\nu) = -\iiint \rho\frac{\partial G(\mathbf{x},\mathbf{y})}{\partial y_j}\,\mathfrak{L}_j(\mathbf{y},\nu)\,d^3\mathbf{y} + \iint \tilde{P}(\mathbf{y}_\beta,\nu)\frac{\partial G(\mathbf{x},\mathbf{y}_\beta)}{\partial n_\beta}d^2\mathbf{y}_\beta, \tag{29}$$

where $\tilde{P}_\beta$ is the pressure difference across the plate. To evaluate this quantity, use will be made of the normal derivative of (29) at a point $\mathbf{x}_\alpha$ on the end plate. As

$$\frac{\partial P(\mathbf{x}_\alpha,\nu)}{\partial n_\alpha} = 0 \tag{30}$$

we obtain

$$\iint \tilde{P}(\mathbf{y}_\beta)\frac{\partial^2 G(\mathbf{x}_\alpha,\mathbf{y}_\beta)}{\partial n_\alpha n_\beta}d^2\mathbf{y}_\beta = \rho\iiint \frac{\partial^2 G(\mathbf{x}_\alpha,\mathbf{y})}{\partial x_i\partial y_j}\,n_{\alpha i}\mathfrak{L}_j(\mathbf{y},\nu)\,d^3\mathbf{y}. \tag{31}$$

3.2 Discretization via the boundary element method and expansion of the surface integrands

Equation (31) is a Fredholm integral equation of first kind. To solve it with respect to the pressure difference $\tilde{P}$, a boundary element method is applied. The surface of the end plate is divided into quadrilateral elements. A simple approach, where $\tilde{P}$ is assumed constant over each element, is applied. This significantly simplifies the evaluation of the normal derivatives, as will be evident in the following.

The last term in equation (29) is thus approximated as follows:

$$\iint \tilde{P}(\mathbf{y}_\beta)\frac{\partial G(\mathbf{x},\mathbf{y}_\beta)}{\partial n_\beta}d^2\mathbf{y}_\beta \approx \sum_e \tilde{P}_{\beta e}\iint \frac{\partial G(\mathbf{x},\mathbf{y}_{\beta e})}{\partial n_\beta}d^2\mathbf{y}_{\beta e}, \tag{32}$$

and the first term in equation (31) as follows:

$$\iint \tilde{P}(\mathbf{y}_\beta)\frac{\partial^2 G(\mathbf{x}_\alpha,\mathbf{y}_\beta)}{\partial n_\alpha n_\beta}d^2\mathbf{y}_\beta \approx \sum_e \tilde{P}_{\beta e}\iint \frac{\partial^2 G(\mathbf{x}_\alpha,\mathbf{y}_{\beta e})}{\partial n_\alpha n_\beta}d^2\mathbf{y}_{\beta e}. \tag{33}$$

In (32) we always have $\mathbf{x} \neq \mathbf{y}_\beta$ and get accordingly

$$\iint \frac{\partial G(\mathbf{x},\mathbf{y}_{\beta e})}{\partial n_\beta}d^2\mathbf{y}_{\beta e} = \iint \frac{e^{ikr_{x\beta}}}{4\pi r_{x\beta}}\left(\frac{1}{r_{x\beta}} - ik\right)\cos(\mathbf{r}_{x\beta},\mathbf{n}_\beta)d^2\mathbf{y}_{\beta e}, \tag{34}$$

where

$$\mathbf{r}_{x\beta} = \mathbf{x} - \mathbf{y}_{\beta e}, \quad r_{x\beta} = |\mathbf{r}_{x\beta}|, \quad \cos(\mathbf{r}_{x\beta},\mathbf{n}_\beta) = \frac{\mathbf{r}_{x\beta}\cdot\mathbf{n}_\beta}{r_{x\beta}}. \tag{35}$$

In (33) we start with evaluation of the derivation with respect to n_α, which gives

$$\begin{aligned}\frac{\partial^2 G}{\partial n_\alpha\partial n_\beta} &= \frac{\partial^2}{\partial n_\alpha\partial n_\beta}\left(\frac{e^{ikr_{\alpha\beta}}}{4\pi r_{\alpha\beta}}\right) \\ &= -\frac{e^{ikr_{\alpha\beta}}}{4\pi r_{\alpha\beta}}\cos(\mathbf{r}_{\alpha\beta},\mathbf{n}_\alpha)\cos(\mathbf{r}_{\alpha\beta},\mathbf{n}_\beta)\left\{\frac{3}{r_{\alpha\beta}^2}(1-ikr_{\alpha\beta}) + (ik)^2\right\} \\ &\quad + \frac{e^{ikr_{\alpha\beta}}}{4\pi r_{\alpha\beta}^3}(1-ikr_{\alpha\beta})\cos(\mathbf{n}_\alpha,\mathbf{n}_\beta).\end{aligned} \tag{36}$$

Two different cases have to be considered: $\mathbf{x}_\alpha \neq \mathbf{y}_{\beta e}$ and $\mathbf{x}_\alpha = \mathbf{y}_{\beta e}$. The first case is straightforward, as $\cos(\mathbf{r}_{\alpha\beta}, \mathbf{n}_\alpha) = \cos(\mathbf{r}_{\alpha\beta}, \mathbf{n}_\beta) = 0$ and $\cos(\mathbf{n}_\alpha, \mathbf{n}_\beta) = 1$; we then obtain

$$\iint \frac{\partial^2 G(\mathbf{x}_\alpha, \mathbf{y}_{\beta e})}{\partial n_\alpha n_\beta} d^2\mathbf{y}_{\beta e} = \iint \frac{\mathrm{e}^{\mathrm{i}kr_{\alpha\beta}}}{4\pi r_{\alpha\beta}^3} (1 - \mathrm{i}kr_{\alpha\beta})\, d^2\mathbf{y}_{\beta e}. \tag{37}$$

For the second case we follow the approach of Terai [19] and consider the limit $\mathbf{x}_\alpha \to \mathbf{y}_{\beta e}$. Let $\mathbf{n} = \mathbf{n}_\alpha = \mathbf{n}_\beta$ and $\mathbf{r} = \mathbf{r}_{\alpha\beta}$. We have then $\mathbf{r} \cdot \mathbf{n} \approx \epsilon$, where ϵ is a small number. Thus $\cos(\mathbf{n}, \mathbf{n}) = 1$, $\cos(\mathbf{r}, \mathbf{n}) = \epsilon/r$, and

$$\begin{aligned}
&\iint \frac{\partial^2}{\partial^2 n} \left(\frac{\mathrm{e}^{\mathrm{i}kr}}{4\pi r}\right) d^2\mathbf{y}_{\beta e} \qquad (38)\\
&= -\iint \frac{\mathrm{e}^{\mathrm{i}kr}}{4\pi} \left[\left\{\frac{3}{r^3}(1 - \mathrm{i}kr) + \frac{(\mathrm{i}k)^2}{r}\right\}\left(\frac{\epsilon}{r}\right)^2 - \frac{1}{r^3}(1 - \mathrm{i}kr)\right] d^2\mathbf{y}_{\beta e}\\
&= -\int_0^{2\pi}\int_\epsilon^{R_e(\theta)} \frac{\mathrm{e}^{\mathrm{i}kr}}{4\pi} \left[\left\{\frac{3}{r^3}(1 - \mathrm{i}kr) + \frac{(\mathrm{i}k)^2}{r}\right\}\left(\frac{\epsilon}{r}\right)^2 - \frac{1}{r^3}(1 - \mathrm{i}kr)\right] r\,dr\,d\theta\\
&= -\frac{1}{4\pi}\int_0^{2\pi} \left[\frac{\mathrm{e}^{\mathrm{i}kr}}{r}\left\{(3 - \mathrm{i}kr)\left(\frac{\epsilon}{r}\right)^2 - 1\right\}\right]_\epsilon^{R_e(\theta)} d\theta\\
&\to \frac{1}{4\pi}\int_0^{2\pi} \frac{\mathrm{e}^{\mathrm{i}kR_e(\theta)}}{R_e(\theta)} d\theta - \tfrac{1}{2}\mathrm{i}k \quad \text{for} \quad \epsilon \to 0.
\end{aligned}$$

3.3 Expansion of the source integrals

Expansion of the derivatives appearing in the source term of (29) gives

$$\begin{aligned}
&\rho \iiint \frac{\partial G(\mathbf{x}, \mathbf{y})}{\partial y_j} \mathfrak{L}_j(\mathbf{y}, \nu)\, d^3\mathbf{y} \qquad (39)\\
&= \rho \iiint \frac{\mathrm{e}^{\mathrm{i}kr}}{4\pi r^3} (1 - \mathrm{i}kr)\,(x_j - y_j)\mathfrak{L}_j(\mathbf{y}, \nu) d^3\mathbf{y},
\end{aligned}$$

where $r = |\mathbf{x} - \mathbf{y}|$. The derivative of this integral in the direction of the normal $\mathbf{n}_\alpha$ takes the form

$$\begin{aligned}
&\rho \iiint \frac{\partial^2 G(\mathbf{x}_\alpha, \mathbf{y})}{\partial x_i \partial y_j} n_{\alpha i} \mathfrak{L}_j(\mathbf{y}, \nu)\, d^3\mathbf{y} = \rho \iiint \frac{\mathrm{e}^{\mathrm{i}kr}}{4\pi r^3} \times \qquad (40)\\
&\times \left[\delta_{ij}(1 - \mathrm{i}kr) - \left((\mathrm{i}k)^2 - \frac{3\mathrm{i}k}{r} + \frac{3}{r^2}\right)(x_i - y_i)(x_j - y_j)\right] n_{\alpha i} \mathfrak{L}_j(\mathbf{y}, \nu) d^3\mathbf{y},
\end{aligned}$$

where δ_{ij} is Kronecker's delta.

3.4 Time-domain expressions

Applying the inverse Fourier transform (22) to (29), we obtain

$$p(\mathbf{x}, t) = p_{\mathrm{vtx}}(\mathbf{x}, t) + \sum_e \iint \frac{1}{4\pi r_{x\beta}} \left(\frac{1}{r_{x\beta}}[\tilde{p}_{\beta e}]_{t_*} + \frac{1}{c_0}\left[\frac{\partial \tilde{p}_{\beta e}}{\partial t}\right]_{t_*}\right) \cos(\mathbf{r}_{x\beta}, \mathbf{n}_\beta) d^2\mathbf{y}_{\beta e}, \tag{41}$$

where

$$p_{\mathrm{vtx}}(\mathbf{x}, t) = -\iiint \frac{\rho}{4\pi r} \left(\frac{1}{r}[L_j]_{t_*} + \frac{1}{c_0}\left[\frac{\partial L_j}{\partial t}\right]_{t_*}\right) \frac{x_j - y_j}{r} d^3\mathbf{y}. \tag{42}$$

In similar fashion, (31) takes, for $\mathbf{x}_\alpha \neq \mathbf{y}_\beta$, the form

$$\frac{\partial p_{\rm vtx}(\mathbf{x}_\alpha,t)}{\partial n_\alpha} + \sum_e \iint \frac{1}{4\pi r_{\alpha\beta}^2}\left(\frac{1}{r_{\alpha\beta}}[\tilde{p}_{\beta e}]_{t_*} + \frac{1}{c_0}\left[\frac{\partial \tilde{p}_{\beta e}}{\partial t}\right]_{t_*}\right) d^2\mathbf{y}_{\beta e} = 0. \tag{43}$$

For $\mathbf{x}_\alpha = \mathbf{y}_\beta$, (31) takes the form

$$\frac{\partial p_{\rm vtx}(\mathbf{x}_\alpha,t)}{\partial n_\alpha} + \sum_e \left([\tilde{p}_{\beta e}]_{t_*}\int_0^{2\pi}\frac{d\theta}{4\pi R(\theta)} + \frac{1}{2c_0}\left[\frac{\partial \tilde{p}_{\beta e}}{\partial t}\right]_{t_*}\right) = 0. \tag{44}$$

In both cases, the first term is

$$\begin{aligned}\frac{\partial p_{\rm vtx}(\mathbf{x}_\alpha,t)}{\partial n_\alpha} = \iiint \frac{n_i}{4\pi}\Bigg[&- \left\{\frac{\delta_{ij}}{r^3} - \frac{3}{r^5}(x_i-y_i)(x_j-y_j)\right\}[L_j]_{t_*} \\ &+ \left\{\frac{\delta_{ij}}{c_0 r^2} - \frac{3}{c_0 r^4}(x_i-y_i)(x_j-y_j)\right\}\left[\frac{\partial L_j}{\partial t}\right]_{t_*} \\ &+ \frac{1}{c_0 r^3}(x_i-y_i)(x_j-y_j)\left[\frac{\partial^2 L_j}{\partial t^2}\right]_{t_*}\Bigg] d^3\mathbf{y}.\end{aligned} \tag{45}$$

3.5 Acoustic feedback model

The velocity at any point $\mathbf{x}$ can be thought of as consisting of two parts: one part from the incompressible 'background flow' (which is modelled by discrete vortices), and one part generated by acoustic pressure fluctuations, that is, by compressibility effects. Clearly the latter contribution is much smaller than the former.

Let $\mathbf{v}(\mathbf{x},t)$ denote the acoustic velocity component. It is related to the acoustic pressure $p(\mathbf{x},t)$ via the linearized Euler equation

$$\rho\frac{\partial \mathbf{v}(\mathbf{x},t)}{\partial t} = -\nabla p(\mathbf{x},t). \tag{46}$$

Applying the Fourier transform (22) to this equation gives

$$\rho\,\mathrm{i}\nu\,\mathbf{V}(\mathbf{x},\nu) = -\nabla P(\mathbf{x},\nu). \tag{47}$$

Equation (29) can be used in evaluating the velocity $\mathbf{V}$ from (47). The theory of vortex sound, represented by the first term on the right hand side of (29), is however only correct if the observation point $\mathbf{x}$ is located in the 'far field', well away from the sound-generating vortex-dominated flow. The sound scattered by the end plate, described by the second term on the right hand side in (29) is of course generated by the preceding vortex sound term, that is, by the nearby vortices. But no far field approximations have been introduced into (29); it is 'exact'. Hence we choose to base the evaluation of acoustic velocity on the scattered pressure field and use the approximation

$$\rho\,\mathrm{i}\nu\,\mathbf{V}(\mathbf{x},\nu) \approx -\nabla P_{\rm scat}(\mathbf{x},\nu), \tag{48}$$

where

$$P_{\rm scat} = (\mathbf{x},\nu) = \iint \tilde{P}(\mathbf{y}_\beta)\frac{\partial G(\mathbf{x},\mathbf{y}_\beta)}{\partial n_\beta} d^2\mathbf{y}_\beta. \tag{49}$$

Inserting (34) into (49), followed by differentiation with respect to x_j ($j = 1,2,3$), we obtain

$$\begin{aligned}\mathbf{V}(\mathbf{x},\nu) \;=\; &\frac{1}{\rho c_0}\sum_e \tilde{P}_{\beta e}\iint \frac{\mathrm{e}^{\mathrm{i}kr_{x\beta}}}{4\pi}\Bigg[\left(-\frac{1}{\mathrm{i}kr_{x\beta}^3} + \frac{1}{r_{x\beta}^2}\right)\times \\ &\times\left(3\cos(\mathbf{r}_{x\beta},\mathbf{n}_\beta)\frac{\mathbf{x}-\mathbf{y}_\beta}{r_{x\beta}} - \mathbf{n}_\beta\right) \\ &- \mathrm{i}k\cos(\mathbf{r}_{x\beta},\mathbf{n}_\beta)\frac{\mathbf{x}-\mathbf{y}_\beta}{r_{x\beta}^2}\Bigg] d^2\mathbf{y}_{\beta e}\end{aligned} \tag{50}$$

Taking the inverse Fourier transform (22) of (50), we obtain

$$\begin{aligned}\mathbf{v}(\mathbf{x},t) &= \frac{1}{4\pi\rho}\sum_e \iint \left[\left(\frac{1}{r_{x\beta}^3}\int_{-\infty}^{t}[\tilde{p}_{\beta e}]_{t_*}\,dt + \frac{1}{c_0\,r_{x\beta}^2}[\tilde{p}_{\beta e}]_{t_*}\right)\times\right. \\ &\times \left(3\cos(\mathbf{r}_{x\beta},\mathbf{n}_\beta)\frac{\mathbf{x}-\mathbf{y}_\beta}{r_{x\beta}} - \mathbf{n}_\beta\right) \\ &+ \left.\frac{1}{c_0^2}\left[\frac{\partial\tilde{p}_{\beta e}}{\partial t}\right]_{t_*}\cos(\mathbf{r}_{x\beta},\mathbf{n}_\beta)\frac{\mathbf{x}-\mathbf{y}_\beta}{r_{x\beta}^2}\right] d^2\mathbf{y}_{\beta e}.\end{aligned} \tag{51}$$

This velocity field is added to the free vortex rings near the nozzle exit. In this way a coupling between the 'vortex field' and the acoustic field (acoustic feedback) is established. It is noted that this approach is in full agreement with Rayleigh's explanation of the 'manner of action', as cited in Section 1.

3.6 Numerical evaluation of the boundary integrals

To evaluate numerically the integrals (37) and (38) over the boundary elements, an isoparametric coordinate transformation is applied, such that the quadrilateral elements are mapped into rectangles [3]. In the global (physical) coordinate system the coordinates $\mathbf{y}_{\beta e}$ within an element can be expressed in terms of the element corner coordinates $(\mathbf{y}_{\beta e})_j, (j = 1,\ldots,4)$ and the isoparametric coordinates $\xi_k, (-1 \le \xi_k \le 1, k = 1,2)$, as

$$\mathbf{y}_\beta = \sum_j N_j(\xi_1,\xi_2)\,(\mathbf{y}_{\beta e})_j, \tag{52}$$

where

$$\begin{aligned} N_1 &= \tfrac{1}{2}(1+\xi_1)(1-\xi_2), \quad N_2 = \tfrac{1}{2}(1+\xi_1)(1+\xi_2), \\ N_3 &= \tfrac{1}{2}(1-\xi_1)(1-\xi_2), \quad N_4 = \tfrac{1}{2}(1-\xi_1)(1-\xi_2). \end{aligned} \tag{53}$$

The surface integral (37) can then be written as

$$\begin{aligned}&\iint \frac{\partial^2 G(\mathbf{x}_\alpha,\mathbf{y}_{\beta e})}{\partial n_\alpha n_\beta} d^2\mathbf{y}_{\beta e} \\ &= \int_{-1}^{1}\int_{-1}^{1} \frac{e^{ikr_{\alpha\beta}(\xi_1,\xi_2)}}{4\pi r_{\alpha\beta}^3(\xi_1,\xi_2)}\{1 - ikr_{\alpha\beta}(\xi_1,\xi_2)\}\,J(\xi_1,\xi_2)\,d\xi_1 d\xi_2,\end{aligned} \tag{54}$$

where $J(\xi_1,\xi_2)$ is the Jacobian of the mapping. Similarly, the final line integral of (38) can be written as

$$\begin{aligned}&\frac{1}{4\pi}\int_0^{2\pi}\frac{e^{ikR_e(\theta)}}{R_e(\theta)}d\theta \\ &= \frac{1}{4\pi}\int_{-1}^{1}\frac{\exp(ik\sqrt{1+\xi_1^2})}{(1+\xi_1^2)^{\frac{3}{2}}}\{J(\xi_1,-1)+J(\xi_1,1)\}\,d\xi_1 \\ &+\frac{1}{4\pi}\int_{-1}^{1}\frac{\exp(ik\sqrt{1+\xi_2^2})}{(1+\xi_2^2)^{\frac{3}{2}}}\{J(-1,\xi_2)+J(1,\xi_2)\}\,d\xi_2.\end{aligned} \tag{55}$$

These integrals, on the right hand sides of (54) and (55), are ideally suited for numerical evaluation via Gaussian quadrature [7].

The expressions given here are for the frequency domain; they are however directly applicable to the time domain solution with $k = 0$.

3.7 Numerical integration of the acoustic equations

The acoustic equations are integrated in time using the trapezoidal method, where the relation between the pressure $\mathbf{p}$ and its time derivative $\dot{\mathbf{p}}$ is given by

$$\mathbf{p}_{n+1} = \mathbf{p}_n + \frac{\Delta t}{2}\left(\dot{\mathbf{p}}_n + \dot{\mathbf{p}}_{n+1}\right). \tag{56}$$

This may be rewritten as

$$\dot{\mathbf{p}}_{n+1} = \frac{2}{\Delta t}\left(\mathbf{p}_{n+1} - \mathbf{p}_n\right) - \dot{\mathbf{p}}_n. \tag{57}$$

Rewriting (43)-(45) into matrix form we obtain

$$\mathbf{C}\dot{\mathbf{p}}_n + \mathbf{K}\mathbf{p}_n = \mathbf{r}_n, \tag{58}$$

where

$$C_{ij} = \begin{cases} -\frac{1}{2}c_0^{-1} & \text{for} \quad i = j, \\ 0 & \text{for} \quad i \neq j, \end{cases} \tag{59}$$

$$K_{ij} = \begin{cases} -\int_0^{2\pi} \frac{d\theta}{4\pi R(\theta)} & \text{for} \quad i = j, \\ -\iint \frac{d^2 y_j}{4\pi r_{ij}^3} & \text{for} \quad i \neq j, \end{cases} \tag{60}$$

and

$$r_j = \frac{\partial p_{\text{vtx}}(\mathbf{x}_j, t)}{\partial n_j}. \tag{61}$$

Inserting (57) into (58), the latter equation may be rewritten into the form of a standard linear equation,

$$\mathbf{K}^{\text{eff}}\mathbf{p}_{n+1} = \mathbf{r}_{n+1}^{\text{eff}}, \tag{62}$$

with

$$\mathbf{K}^{\text{eff}} = \frac{2}{\Delta t}\mathbf{C} + \mathbf{K}, \tag{63}$$

and

$$\mathbf{r}_{n+1}^{\text{eff}} = \mathbf{r}_{n+1} + \mathbf{C}\left(\frac{2}{\Delta t}\mathbf{p}_n + \dot{\mathbf{p}}_n\right). \tag{64}$$

Equation (62) is solved with respect to $\mathbf{p}_{n+1}$ at each time step. Following this, $\dot{\mathbf{p}}_{n+1}$ is updated using (57). But, as 'numerical noise' in the velocities is unavoidable by the discrete vortex method, the use of (57) may amplify this 'noise' to an unacceptable level. A smoother and more useful pressure time series can be obtained by differentiating a least-square fit of a number of consecutive points on the 'pressure curve', as suggested by Lanczos [7]. The formula for the general case of smoothing by use of K neighbors on both sides of the point where the derivative is wanted is given by

$$\frac{\partial \mathbf{p}(t)}{\partial t} = \left(\sum_{k=-K}^{K} k\mathbf{p}(t + k\Delta t)\right) \Big/ \left(2\sum_{k=1}^{K} k^2 \Delta t\right). \tag{65}$$

As values ahead are needed, the pressure evaluation must lag K time steps after the actual state. If $K = 2$, for example, the formula is

$$\frac{\partial \mathbf{p}(t - 2\Delta t)}{\partial t} = \frac{1}{10\Delta t}\{-2\mathbf{p}(t - 4\Delta t) - \mathbf{p}(t - 3\Delta t) + \mathbf{p}(t - \Delta t) + 2\mathbf{p}(t)\}, \tag{66}$$

or, with the notation used in this section,

$$\dot{\mathbf{p}}_{n-2} = \frac{1}{10\Delta t}\left(-2\mathbf{p}_{n-4} - \mathbf{p}_{n-3} + \mathbf{p}_{n-1} + 2\mathbf{p}_n\right). \tag{67}$$

3.8 Test of the boundary element method

The scattering of a plane, harmonic wave by a thin rigid disk, of radius a, is considered as a test case for the boundary element method. An analytical solution has been derived by Noble [12]. The incoming pressure wave, incident normally on the disk, is given by $P_i = \exp(-ikz)$. The scattered pressure wave can be expressed as

$$P_s(r,\theta,\lambda) = \frac{2}{\pi}k^2a^3\sum_{n=0}^{\infty}\frac{(-1)^n(\lambda a)^{2n}}{1\cdot 3\cdots(4n+1)}X_{2n+\frac{3}{2}}(\lambda a)P_{2n+1}(\cos\theta)\left(\frac{2\lambda}{\pi r}\right)^{\frac{1}{2}}K_{2n+\frac{3}{2}}(\lambda r), \qquad (68)$$

where $\lambda = -ik$. The functions $X_{2n+\frac{3}{2}}(\lambda a)$ are defined in Ref. [12] in terms of a recursive formula. The terms necessary to evaluate the pressure to order $(\lambda a)^4$ are

$$\begin{aligned} X_{\frac{3}{2}}(\lambda a) &= \frac{1}{3} - \frac{4}{75}(\lambda a)^2 + \frac{2}{27\pi}(\lambda a)^3 + \frac{1}{5\cdot 7^2}(\lambda a)^4 + \cdots \qquad (69)\\ X_{\frac{7}{2}}(\lambda a) &= \frac{1}{5} - \frac{2}{3^2\cdot 7}(\lambda a)^2 + \cdots, \quad X_{\frac{11}{2}}(\lambda a) = \frac{1}{7} + \cdots \end{aligned}$$

The functions $P_{2n+1}(\theta)$ are Legendre polynomials, given by

$$\begin{aligned} P_1(\cos\theta) &= \cos\theta, \qquad (70)\\ P_2(\cos\theta) &= \tfrac{1}{8}(3\cos\theta + 5\cos 3\theta),\\ P_3(\cos\theta) &= \tfrac{1}{128}(30\cos\theta + 35\cos 3\theta + 63\cos 5\theta),\\ &\vdots \end{aligned}$$

Finally, the functions $K_{2n+\frac{3}{2}}(\lambda r)$ are modified Bessel functions of the second kind.

The intensity of the scattered sound field as function of the angle θ, computed via the boundary element method and via the analytical expression (68), is shown in a polar plot in Fig. 2(a). The diameter of the disk is 1 m, the frequency is 10 Hz, and the distance from the center of the plate to the observation point r is 10 m. The agreement is very good for relatively small values of ka, i.e. for low frequencies, as considered here. [The agreement is less good for higher frequencies; it appears that more terms in series for the X-functions of (69) are then needed.] The plot also illustrates a pure dipole behavior of the plate for low frequencies. This can also be seen directly from (68)-(70). Fig. 2(b) shows the boundary element grid used; the number of elements is 1152.

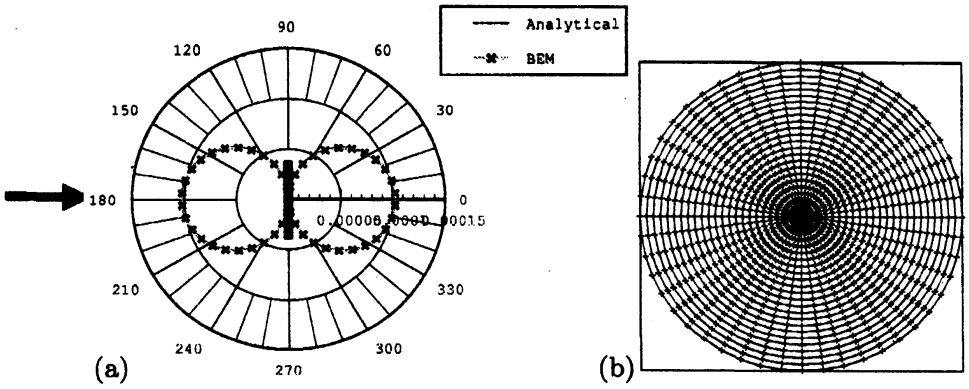

Figure 2: (a) Layout of a thin rigid disk and the incoming wave, and intensity distribution of the scattered wave (polar diagram). (b) The boundary element grid used in the computation.

4 Numerical example

Computations have been carried out for data corresponding to an experimental rig with nozzle and end plate hole diameter $d_0 = 2r_0 = 50\,\text{mm}$ [11]. The outer diameter of the end plate is 250 mm. The gap length ℓ is 50 mm, e.g., equal to d_0. The mean velocity u_0 of the air-jet is 10 m/s. At 20 °C this corresponds to a Reynolds number $Re = u_0\, d_0/\nu \approx 3.3 \times 10^4$ and a Mach number $M = u_0/c_0 \approx 0.03$, where the speed of sound $c_0 = 340$ m/s and the kinematic viscosity $\nu = 1.5 \times 10^{-5}$ m^2/s. The initial vortex core radii $\sigma_j = 0.275 r_0$. A number of side view 'snapshots' of the jet during one period of the oscillations are shown in Fig. 3. The computed fundamental frequency $f_0 \approx 190$ Hz, which is quite close to the experimentally observed value of 196 Hz.

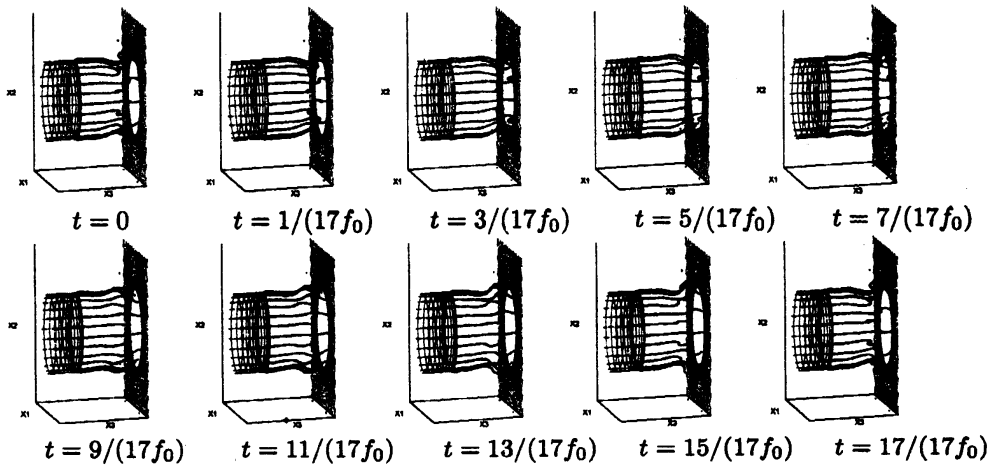

Figure 3: Side view of the jet during one period of oscillation.

Velocity fluctions in the shear layer are illustrated in Fig. 4(a). The data have been recorded $0.2d_0$ away from the end plate. Part (b) of the figure shows the to part (a) corresponding frequency spectrum (given in dB, using $5\,\text{m}\,\text{s}^{-1}$ as reference velocity). The level at the characteristic frequency f_0 is in good agreement with the experimentally recorded value [11]. The experimental spectrum contains however less 'noise' and exhibits distinct higher harmonics $(2f_0, 3f_0, \ldots)$.

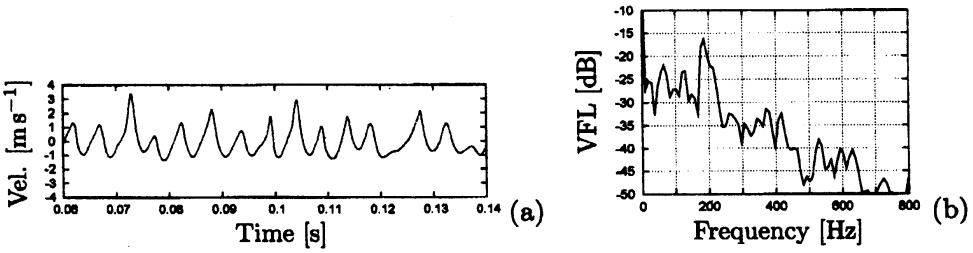

Figure 4: (a) Velocity fluctuations in the shear layer at a distance $0.2d_0$ from the end plate. (b) The corresponding frequency spectrum.

5 Proper orthogonal decomposition analysis

5.1 Description of the method

Proper orthogonal decomposition (POD) is a method for extracting coherent structures from experimental or computational data [4]. By coherent structures is meant fundamental fluid modes, containing a concentration of vorticity and/or responsible for the major part of energy transport.

The velocity field $\mathbf{u}(\mathbf{x},t)$ is recorded at N grid points $\mathbf{x}_1,\ldots,\mathbf{x}_N$ and at M times $t_1,\ldots,t_M$,

$$\mathfrak{U}(\mathbf{x},\mathbf{t}) = \begin{pmatrix} \mathbf{u}(\mathbf{x}_1,t_1) & \mathbf{u}(\mathbf{x}_2,t_1) & \cdots & \mathbf{u}(\mathbf{x}_N,t_1) \\ \mathbf{u}(\mathbf{x}_1,t_2) & \mathbf{u}(\mathbf{x}_2,t_2) & \cdots & \mathbf{u}(\mathbf{x}_N,t_2) \\ \vdots & \vdots & \ddots & \vdots \\ \mathbf{u}(\mathbf{x}_1,t_M) & \mathbf{u}(\mathbf{x}_2,t_m) & \cdots & \mathbf{u}(\mathbf{x}_N,t_M) \end{pmatrix}. \tag{71}$$

The POD method determines a set of orthogonal vector functions $\varphi_n(\mathbf{x})$ from $\mathfrak{U}(\mathbf{x},\mathbf{t})$, such that the expansion of $\mathbf{u}(\mathbf{x},t)$ in terms of these functions,

$$\mathbf{u}_N(\mathbf{x},t) = \sum_{n=1}^{N} a_n(t)\varphi_n(\mathbf{x}), \tag{72}$$

has the smallest error, in the sense that

$$\langle \|\mathbf{u}_N - \mathbf{u}\|^2 \rangle \rightarrow \min, \tag{73}$$

where $\|\cdot\|$ denotes the L^2-norm, and $\langle\cdot\rangle$ denotes averaging.

The determination of the POD modes φ_n involves, in the so-called direct method, the solution of an $N \times N$ eigenvalue problem.

Often the number of grid points $N \gg M$, the number of temporal points. This is taken into advantage in the 'method of snapshots', where the POD modes φ_n are written as a linear combination of the M 'snapshots',

$$\varphi(\mathbf{x}) = \sum_{m=1}^{M} c_m\, \mathbf{u}(\mathbf{x},t_m). \tag{74}$$

Texts on POD, e.g. [4], show that the constants c_m can be determined by solving the $M \times M$ symmetric eigenvalue problem

$$\sum_{m=1}^{M} \frac{1}{M}\, \mathbf{u}_n \cdot \mathbf{u}_m\, c_m = \lambda\, c_n, \quad n = 1,\ldots,M. \tag{75}$$

5.2 Numerical example

Velocities are recorded at 51 × 101 grid points, as shown in Fig. 5. Snapshots are taken over 10 flow-oscillation periods, with 8 snapshots in each period. Thus with $N = 5151$ and $M = 80$, it is clearly of advantage to use the method of snapshots. The modal functions $\varphi_1,\ldots,\varphi_4$ are shown in Fig. 6. It should be noted that the mean velocity $\mathbf{u}_0(\mathbf{x})$ was subtracted before (75) was set up and solved. Thus, rather than (72), the expansion

$$\mathbf{u}_N(\mathbf{x},t) = \mathbf{u}_0(\mathbf{x}) + \sum_{n=1}^{N} \tilde{a}_n(t)\varphi_n(\mathbf{x}) \tag{76}$$

is considered. Mode 1 has a mean-flow-like appearance, while modes 2, 3, and 4 are characterized by the appearance of one vortex, two vortices, and three vortices, respectively. It seems likely

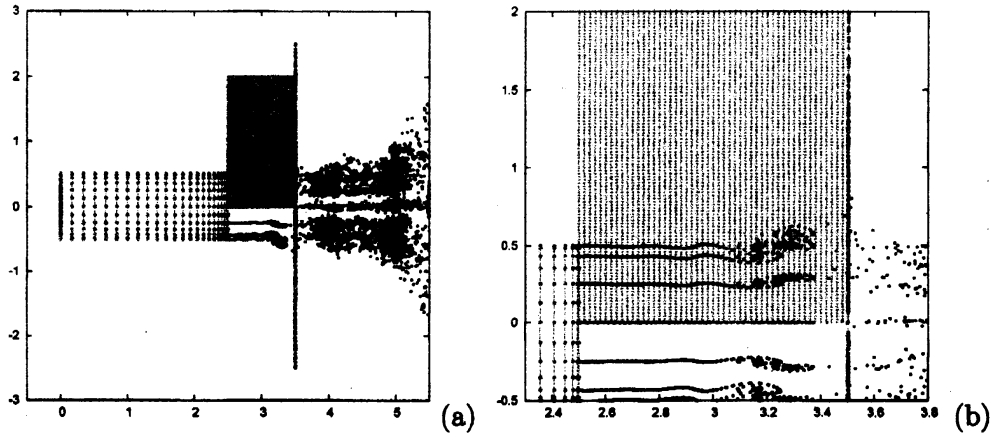

Figure 5: The 51×101 grid used for obtaining velocity snapshots. (a) The whole computational system. (b) Zoom-in around the grid.

that the mentioned phenomenon of mode jumps is related to the mutual balance between these fundamental modes. This can, we believe, be verified by a low-dimensional analysis based on the Euler equations, discretized via the Galerkin method, with the POD modes as basis functions. Rowley *et al.* have applied such an approach to the problem of self-sustained oscillations in the flow over a rectangular cavity, and found that the results of a full simulation could be captured by the Galerkin approximation using just four modes.

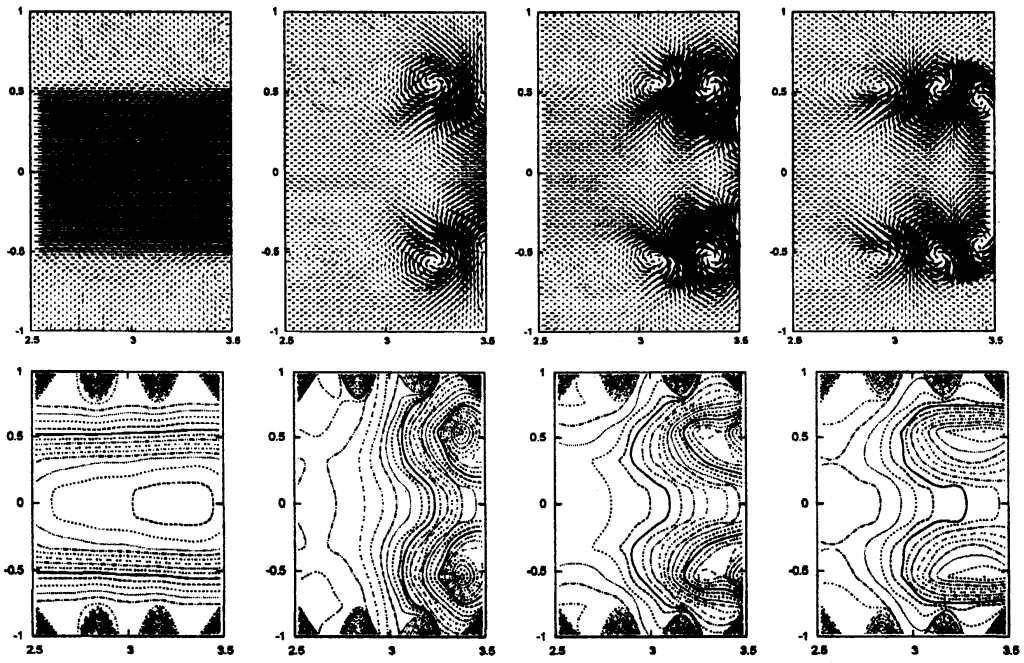

Figure 6: POD modes 1 through 4 (from left to right). The figures in the upper row show velocity vectors; those in the lower row are iso-velocity contour plots. The coordinates are as in Fig. 5, i.e. the nozzle exit is at abscissa 2.5; the end plate at 3.5.

This appears to apply to the present problem as well. The eigenvalues λ_m of (75) are shown in Fig. 7. These eigenvalues represent twice the kinetic energy of the corresponding mode φ_m. It is seen that the magnitude falls off rapidly with increasing mode number. Thus only the first four or five modes will be of significance in governing the dynamics of the system.

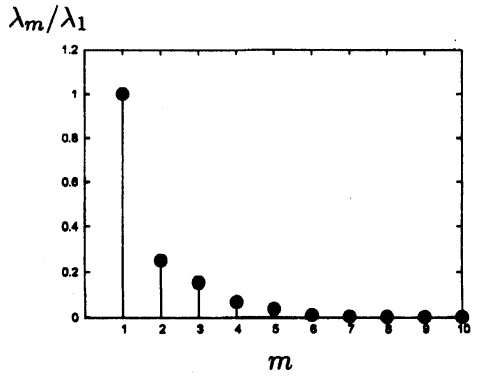

Figure 7: Eigenvalues related to the POD modes.

Acknowledgement

The support of the present project through a JSPS Grant-in-Aid for Scientific Research (No. 18560152) is gratefully acknowledged.

References

[1] W.T. Ashurst, E, Meiburg, Three-dimensional shear layers via vortex dynamics, *J. Fluid Mech.* 189 (1988), 87-116.

[2] R.C. Chanaud, A. Powell, Some experiments concerning the hole and ring tone, *J. Acoust. Soc. Am.* 37 (1965) 902-911.

[3] R.D. Cook, D.S. Malkus, M.E. Plesha, *Concepts and Applications of Finite Element Analysis*, John Wiley & Sons, New York, 1989.

[4] P. Holmes, J.L. Lumley, G. Berkooz, *Turbulence, Coherent Structures, Dynamical Systems and Symmetry*, Cambridge University Press, Cambridge UK, 1996.

[5] M. S. Howe, *Theory of Vortex Sound*, Cambridge University Press, Cambridge UK, 2003.

[6] J. Katz, A. Plotkin, *Low-Speed Aerodynamics*,Cambridge University Press, Cambridge UK, 2001.

[7] C. Lanczos, *Applied Analysis*, Dover Publications, New York, 1988.

[8] M.A. Langthjem, M. Nakano, A numerical study on the influence of non-axisymmetric flow perturbations on the hole-tone feedback cycle, *RIMS Kôkyûroku* 1543 (2007), 21-30.

[9] A. Leonard, Computing three-dimensional incompressible flows with vortex elements, *Annu. Rev. Fluid Mech.* 17 (1985), 523-559.

[10] P.M. Morse, K.U. Ingard, *Theoretical Acoustics*, Princeton University Press, Princeton NJ, 1986.

[11] M. Nakano, D. Tsuchidoi, K. Kohiyama, A. Rinoshika, K. Shirono, Wavelet analysis on behavior of hole-tone self-sustained oscillation of impinging circular air jet subjected to acoustic excitation, (In Japanese) *Kashikajouhou* 24 (2004), 87-90.

[12] B. Noble, *Methods based on the Wiener-Hopf Technique for the Solution of Partial Differential Equations*, Chelsea Publishing Company, New York, 1988.

[13] I.G. Petrovsky, *Lectures on Partial Differential Equations*, Dover Publications, New York, 1991.

[14] A. Pikovsky, M. Rosenblum, J. Kurths, *Syncronization: A Universal Concept in Nonlinear Sciences*, Cambridge University Press, Cambridge UK, 2001.

[15] Lord Rayleigh, *The Theory of Sound*, Vol. II, Dover Publications, New York, 1945.

[16] Rockwell, D., Naudascher, E., Self-sustained oscillations of impinging free shear layers. *Annu. Rev. Fluid Mech.* 11 (1979) 67-94.

[17] Rockwell, D., Oscillations of impinging shear layers. *AIAA J.* 21 (1983) 645-664.

[18] C.W. Rowley, T. Colonius, R.M. Murray, Model reduction for compressible flows using POD and Galerkin projection, *Physica D* 189 (2004), 115-129.

[19] T. Terai, On calculation of sound fields around three dimensional objects by integral equation methods, *J. Sound Vib.* 37 (1980) 71-100.